Ultrafast Photoinduced Charge Separation Resulting from Self-assembly of a Green Perylene-based Dye into π-Stacked Arrays

Michael J. Fuller, Louise E. Sinks, Boris Rybtchinski, Jovan M. Giaimo, Xiyou Li, and Michael R. Wasielewski*

Department of Chemistry and Center for Nanofabrication and Molecular Self-Assembly, Northwestern University, Evanston, Illinois 60208-3113

Received: November 14, 2004; In Final Form: December 7, 2004

Condensation of 3,4,5-tris(*n*-dodecyloxy)aniline with the green chromophore 1,7-bis(*N*-pyrrolidinyl)perylene-3,4;9,10-tetracarboxylic dianhydride yields *N*,*N*′-bis(3,4,5-tris(*n*-dodecyloxy)phenyl)-1,7-bis(*N*-pyrrolidinyl)-perylene-3,4;9,10-bis(dicarboximide), 5PDI-TAP, which absorbs light strongly from 550 to 750 nm. 5PDI-TAP dissolves readily in methylcyclohexane (MCH), resulting in self-assembly into *H*-aggregates. Small-angle X-ray scattering data obtained on 10^{-4} M solutions of 5PDI-TAP in MCH show that the aggregates are π-stacked monodisperse pentamers. Femtosecond transient absorption spectroscopy on solutions of $(5PDI\text{-}TAP)_5$ in MCH shows evidence of charge separation occurring with $\tau \leq 150$ fs between adjacent stacked members of 5PDI-TAP within the pentamer followed by charge recombination with $\tau = 860$ ps. Transmission electron microscopy of 5PDI-TAP films cast from solution show isolated bundles of columnar aggregates. $(5PDI\text{-}TAP)_n$ is a potentially useful material for organic photovoltaics because efficient photoinduced charge generation is an intrinsic property of the assembly.

Recent research has focused on the self-assembly of organic molecules into supramolecular architectures in order to develop new materials for organic photonics and electronics.[1−16] In organic photovoltaic (OPV) materials, optimal performance requires both efficient charge generation and long distance charge transport.[11] Composite OPV materials containing discotic liquid crystal (LC) donors and acceptors have been examined with a view toward improving charge transport characteristics by increasing the electronic coupling between molecules that self-assemble via π-stacking.[1,3−7,16] For example, photoactive discotic LCs prepared from perylene-3,4;9,10-bis(dicarboximide) and coronene derivatives have been reported recently.[1,8−10,12−15] In addition, perylene-3,4;9,10-bis(dicarboximide) derivatives with long-chain 3,4,5-trialkoxyphenyl (TAP) groups attached either directly to the imide nitrogen atoms[8] or indirectly to it with an intervening methylene group[7] have been shown to form *J*-aggregates, when dissolved in methylcyclohexane (MCH).

The electronic properties of perylene-3,4;9,10-bis(dicarboximide) chromophores can be tailored by changing substituents on the perylene chromophores, yielding a family of n-type[17] and p-type materials.[18,19] We have previously reported a series of green chromophores with *N*-cycloalkylamino substituents attached to the 1 and 7 positions of the perylene core.[18,19] In particular, 1,7-bis(*N*-pyrrolidinyl)perylene-3,4;9,10-bis(dicarboximide), 5PDI, displays an intense optical absorption band near 700 nm, which is significantly red shifted relative to the 550 nm absorbance of the corresponding 1,7-diphenoxy derivatives (PDI). In addition, we recently presented direct evidence using ultrafast transient absorption spectroscopy for symmetry breaking in the lowest excited singlet state of a symmetric

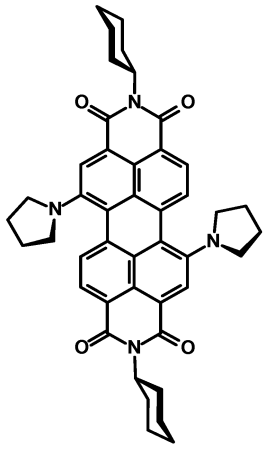

5PDI

cofacial 5PDI dimer (*cof*-$5PDI_2$), which results in the quantitative production of a $5PDI^{\bullet+}-5PDI^{\bullet-}$ radical ion pair in the low-polarity solvent toluene with $\tau = 0.52$ ps followed by charge recombination to ground state with $\tau = 220$ ps.[20] Photoexcitation of chromophoric dimers constrained to a symmetric π-stacked geometry by their molecular structure usually produces excimers independent of solvent polarity,[21] while dimers with perpendicular edge-to-edge π systems have been shown to undergo excited-state symmetry breaking in polar solvents leading to intradimer charge separation.[22,23] An important possible exception is the special pair of bacteriochlorophyll molecules that acts as the primary electron donor in bacterial photosynthetic reaction center proteins. The electronic excited state of the special pair is thought to have significant charge resonance character,[24−27] which may result in symmetry breaking that leads

* Address correspondence to this author. Phone: (847) 467-1423. E-mail: wasielew@chem.northwestern.edu.

10.1021/jp044796q CCC: $30.25
Published on Web 01/21/2005

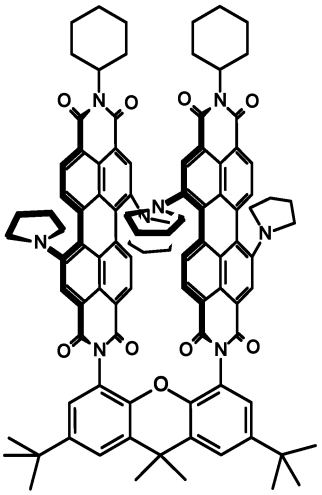

***cof*-5PDI$_2$**

to unidirectional electron transfer using one of the two sets of redundant electron acceptors within the protein. We recently reported on a noncovalent artificial photosynthetic array consisting of four PDI chromophores covalently attached to a 5PDI core, which was found to self-assemble into dimers, (5PDI−PDI$_4$)$_2$, in toluene and THF.[28] Energy transfer from ^{1*}PDI to 5PDI was observed with $\tau = 21$ ps, followed by excited-state symmetry breaking between the two noncovalent stacked 5PDI molecules to produce 5PDI$^{\bullet+}$−5PDI$^{\bullet-}$ with $\tau = 7$ ps. Electron transfer occurred only in the self-assembled dimer, and did not occur in the disassembled monomer.

In this work, we present results on *N*,*N*′-bis(3,4,5-tris(*n*-dodecyloxy)phenyl)-1,7-bis(*N*-pyrrolidinyl)perylene-3,4:9,10-bis(dicarboximide) (5PDI-TAP), which self-assembles into

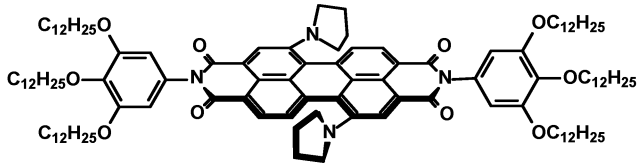

5PDI-TAP

ordered aggregates in nonpolar solvents. Photoexcitation of the self-assembled strongly interacting cofacial 5PDI-TAP molecules results in quantitative charge separation within the aggregates, similar to that observed in *cof*-5PDI$_2$ and (5PDI−PDI$_4$)$_2$. Thus electron transfer arises as a consequence of formation of the self-assembled structure, making (5PDI-TAP)$_n$ a potentially useful OPV material because efficient charge generation is an intrinsic property of the assembly.

Experimental Section

Proton nuclear magnetic resonance spectra were recorded on a Varian Mercury-400 MHz or a Varian INOVA-500 MHz NMR spectrometer using TMS as an internal standard. Laser desorption mass spectra were obtained with a PE Voyager DE-Pro MALDI-TOF mass spectrometer using dithranol as a matrix. Solvents and reagents were used as received except for MTHF, which was purified by passing it through a column of basic alumina immediately before use, and toluene and THF, which were purified by passing them through a series of CuO and alumina columns (GlassContour). Flash and thin-layer chromatography was performed using Sorbent Technologies (Atlanta, GA) silica gel. Merck silica gel 60 was used for column chromatography.

1,7-Bis(pyrrolidin-1-yl)perylene-3,4;9,10-tetracarboxydianhydride, 5PDA. *N*-Cyclohexyl-1,7-bis(pyrrolidin-1-yl)-perylene-3,4-imide-9,10-anhydride (125 mg, (0.18 mmol)[19] and 489 mg of (8.72 mmol) potassium hydroxide were added to a 25 mL round-bottom flask containing 10 mL of 2-propanol. The solution was sonicated for 1 min. The reaction mixture was heated to reflux for 30 min and then slowly poured into 50 mL of glacial acetic acid with vigorous stirring. After stirring for 10 min the product was extracted with 75 mL of chloroform. The chloroform layer was washed with three 100 mL portions of water, dried over sodium sulfate, filtered, and rotary evaporated to give a green solid (59 mg, 0.11 mmol, 61% yield). ^{1}H NMR δ ($CDCl_3$): 8.47 (s, 2H), 8.43 (d, $J = 8.0$ Hz, 2H), 7.60 (d, $J = 8.0$ Hz; 2H), 3.75 (br s, 4H), 2.84 (br s, 4H), 2.14 (br s, 4H), 2.02 (br s, 4H). MS: 531.11 (M + H) (calcd 530.15).

***N*,*N*′-(3,4,5-Tris(*n*-dodecyloxy)phenyl)-1,7-bis(pyrrolidin-1-yl)perylene-3,4;9,10-bis(dicarboximide), 5PDI-TAP.** 5PDA (36 mg, 0.068 mmol) and 3,4,5-tris(*n*-dodecyloxy)aniline[29] (0.219 g, 0.34 mmol) were combined with excess imidazole (0.360 g) and 4 mL of toluene in a 20 mL round-bottom flask. The reaction mixture was sonicated to complete dissolution and was heated to reflux with stirring for 14 h under nitrogen. The solvent was evaporated under vacuum, and the dried reaction contents were taken up in 75 mL of chloroform. The chloroform extract was washed three times with 50 mL of water, dried over anhydrous sodium sulfate, and evaporated to dryness. The crude product was chromatographed on a silica column using a mixture of 60% hexane, 10% acetone, and 30% chloroform as the eluent to yield 5PDI-TAP (0.071 g, 59% yield). mp 92−94 °C. ^{1}H NMR ($CDCl_3$) δ: 8.53 (s, 2H), 8.49 (d, $J = 8.0$ Hz, 2H), 7.75 (d, $J = 8.0$ Hz, 2H), 6.53 (s, 4H), 4.04 (t, $J = 6.4$ Hz, 4H), 3.96 (t, $J = 6.3$ Hz, 8H), 3.77 (unr t, 4H), 2.85 (unr t, 4H), 2.09 (unr quintet, 4H), 2.01 (unr quintet, 4H), 1.80 (quintet, $J = 7.1$ Hz, 12H), 1.49 (unr multiplet, 108H), 0.87 (t, $J = 6.6$ Hz, 18H). MS: 1785.0 (calcd 1785.3).

Small-angle X-ray scattering measurements were carried out using the undulator beam line 12-ID at the Advanced Photon Source (APS), Argonne National Laboratory. The X-ray scattering instrument utilized a double-crystal Si(111) monochromator and a two-dimensional mosaic CCD detector.[30] The X-ray wavelength was set at $\lambda = 1.0$ Å, and the sample-to-detector distance was adjusted to achieve scattering measured across the $0\ \text{Å}^{-1} < q < 0.5\ \text{Å}^{-1}$ region, where $q = (4\pi/\lambda)\sin\theta$; λ is the X-ray wavelength and 2θ is the scattering angle. A quartz capillary (0.2 mm diameter) was used as the sample container. All the samples were filtered through 200 nm PTFE filters prior to the measurements. Three measurements were made for each sample and average intensity was calculated; solvent scattering was systematically measured and subtracted from the sample spectrum as a background. In the low resolution scattering region below $q = 0.1\ \text{Å}^{-1}$, the scattering follows the Guinier relationship, $I(q) = I(0)\exp(-q^2R_g^2/3)$, parametrized in terms of the forward scattering amplitude, $I(0)$, and the radius of gyration, R_g. The linearity of the Guinier plot is a measure of the monodispersity of the aggregate.[31,32]

Pair distance distribution functions (PDF) were determined from the scattering patterns using indirect Fourier transforms[33] with the program GNOM.[33,34] The reconstruction of the aggregate shape was done with the program DAMMIN[35] using as an input a GNOM ".out" file containing experimental data. To obtain a more reliable solution, several independent DAM-

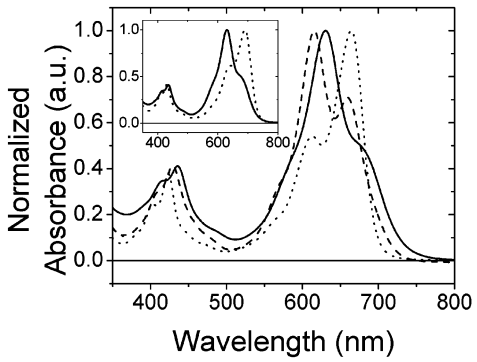

Figure 1. Electronic absorption spectra of 5PDI-TAP (—), *cof*-5PDI$_2$ (---), and 5PDI (•••) in MCH. Inset: electronic absorption spectrum of 5PDI-TAP in toluene (---) and MCH (—).

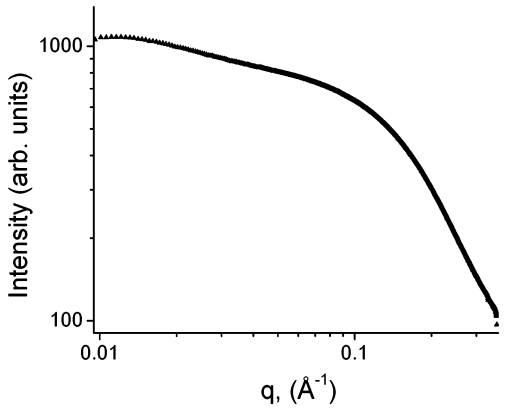

Figure 2. Experimental scattering data for 5PDI-TAP in MCH (10^{-4} M).

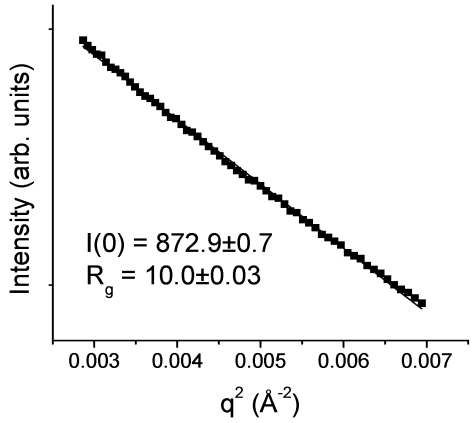

Figure 3. Guinier fit (solid line) for 5PDI-TAP in MCH (10^{-4} M).

MIN runs were performed, and the resulting solutions were averaged using the DAMAVER program package.[36]

Transmission electron microscopic (TEM) observations were conducted using a Hitachi H8100 (200 kV) electron microscope. The TEM grid was a copper grid covered with an ultrathin carbon film (Ted Pella, Inc.).

Cyclic voltammetry measurements were performed in butyronitrile solution containing 0.1 M tetra-*n*-butylammonium hexfluorophosphate ($TBAPF_6$) electrolyte using a CH Model 622 electrochemical workstation. A 1.0 mm diameter platinum disk electrode, platinum wire counter electrode, and Ag/Ag_xO reference electrode were employed. The ferrocene/ferricenium couple was used as an internal reference for all measurements.

Steady-state absorption and emission spectra were performed on a Shimadzu 1601 UV/vis spectrophotometer. A 10 mm quartz cuvette was used for both the absorption and fluorescence measurements, and the optical density at λ_{max} for the fluorescence measurements was maintained at 0.1 ± 0.05 to avoid reabsorption artifacts. Femtosecond transient absorption measurements were carried out using an amplified Ti:sapphire, 1 kHz repetition rate laser system and techniques described in detail earlier.[37] The total instrument response function for the pump−probe experiments was 130 fs. Cuvettes with a 2 mm path length were used, and the samples were irradiated with 0.5−1.0 μJ per pulse focused to a 200 μm spot. The optical density at λ_{max} was typically 0.4−0.8. Kinetic analyses were performed at several wavelengths using a Levenberg−Marquardt nonlinear least-squares fit to a general sum-of-exponentials function with an added Gaussian to account for the finite instrument response.

Results and Discussion

The ground-state absorption spectrum of 10^{-5}M 5PDI-TAP in MCH is given in Figure 1 and shows features indicative of *H*-aggregate formation. The spectrum is compared with those of *cof*-5PDI$_2$ and a monomeric 5PDI reference compound bearing *N*-cyclohexyl substituents that does not aggregate in MCH. 5PDI-TAP displays an absorption maximum at 630 nm in MCH with a weaker shoulder near 670 nm. For comparison, the absorption spectrum of 5PDI in MCH has maximum absorbance at 665 nm and is very similar to that in toluene. In MCH, the optical absorption spectrum of *cof*-5PDI$_2$ shows a peak at 615 nm and a shoulder at 660 nm, and very closely resembles that of 5PDI-TAP. The 5PDI units in *cof*-5PDI$_2$ are geometrically constrained to a stacked, cofacial orientation with an interplanar distance of 3.7 Å.[20] Enhancement of the first vibronic band in the absorption spectrum of both *cof*-5PDI$_2$ and 5PDI-TAP is indicative of molecular aggregation with parallel transition dipoles between adjacent 5PDI molecules (*H*-aggregates).[38] However, the relative intensities of the 630 and 670 nm bands of 5PDI-TAP in MCH do not indicate the actual size of the aggregates formed. A comparison of the optical absorption spectrum of 5PDI-TAP in MCH with that obtained in toluene (inset, Figure 1) shows that *H*-aggregates do not form in toluene at low concentrations (10^{-5} M). Spectra similar to that obtained in MCH are observed for 5PDI-TAP dissolved in other saturated alkanes, such as heptane, at 10^{-5} M (data not shown).

To estimate the 5PDI-TAP aggregate size and shape in MCH solution, we performed small-angle X-ray scattering (SAXS) measurements using a high-flux synchrotron source (Advanced Photon Source (APS) at Argonne National Laboratory; see Experimental Section). The scattering intensity is a function of the scattering vector, q, which is related to the scattering angle 2θ by the relationship $q = (4\pi/\lambda) \sin \theta$, where λ is the X-ray wavelength; see Figure 2. In the low resolution scattering region below $q = 0.1$ Å^{-1}, the calculated scattering follows the Guinier relationship[31] $I(q) = I(0) \exp(-q^2R_g^2/3)$, parametrized in terms of the forward scattering amplitude, $I(0)$, and the radius of gyration, R_g. A Guinier plot of the data for 5PDI-TAP is presented in Figure 3. The data for 5PDI-TAP show essentially linear plots in MCH in the range 0.05 Å^{-1} < q < 0.09 Å^{-1} (0.003 Å^{-2} < q^2 < 0.007 Å^{-2}), indicating that the MCH aggregates are monodisperse.[31,32] R_g is not directly related to the molecular structure, but is the electron-density-contrast weighted sum of the squares of the atomic distances from the center of mass, and hence depends on a combination of factors including electron density contrast with the solvent and structure of the solvent-excluded and solvent-associated layers.[39,40] Thus, for 5PDI-TAP in MCH $R_g = 10.0 \pm 0.1$ Å, which indicates

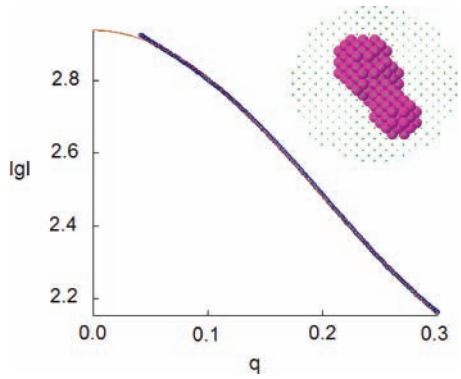

Figure 4. Fit of calculated (red line) and experimental (blue scatter) intensity pattern for 5PDI-TAP aggregate. Inset: top view of the reconstructed aggregate.

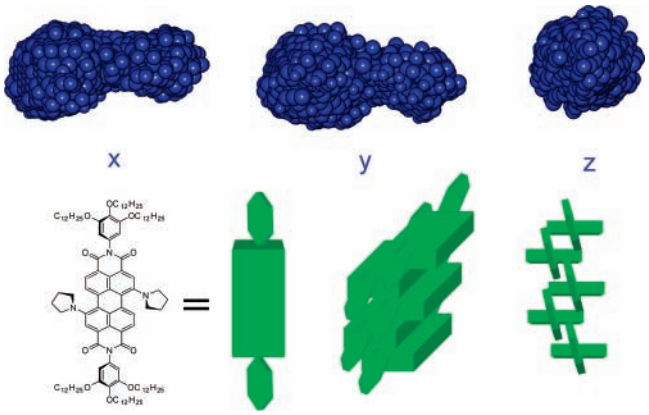

Figure 5. 5PDI-TAP aggregate structure in solution (10^{-4} M) with dimensions 3.6 × 2.0 × 1.8 nm. Model of the arrangement of $(5PDI\text{-}TAP)_5$ based on the steric demand of the 3,4,5-trialkoxyphenyl groups, which are 78° out-of-plane with the 5PDI core chromophore. Lateral slippage of 5PDI-TAP cores still permits *H*-aggregation.

that it forms small aggregates in MCH. The monodisperse nature of aggregates based on PDI derivatives at a particular concentration in solution is intriguing because we have observed this in several cases using SAXS in solution.[41,42] A likely reason for the formation of monodisperse aggregates has to do with the limited solubility of higher aggregates. The sizes of the aggregates increase until only aggregates of a specific final size are soluble at a given concentration.

The monodispersity of the 5PDI-TAP aggregates allows an analysis of the scattering data using a simulated annealing procedure.[36] This analysis shows that the dimensions of the 5PDI-TAP aggregates are roughly 3.6 × 2.0 × 1.8 nm (Figures 4 and 5), and the R_g value for the reconstructed aggregates is 9.9 ± 0.1 Å, which corresponds well to the R_g value of 10.0 ± 0.1 Å obtained by experiment. Assuming a characteristic interchromophore distance of 3.5−3.7 Å, which gives rise to the observed exciton coupling, the dimensions and shape of the reconstructed aggregate suggest that a cofacially stacked 5PDI-TAP pentamer, Figure 5, is formed in MCH. It should be noted that the TAP alkyl chains do not appear to contribute significantly to the overall dimensions of the aggregate. This is most probably due to their highly flexible nature and poor scattering contrast with the hydrocarbon solvent (MCH).

The energy-minimized ground-state structure of 5PDI-TAP calculated using the PM3 formalism finds that the planes of the TAP phenyl groups attached to the imides are rotated 78° relative to the plane of the imide.[43] The proposed stacking motif shown in Figure 5, where the alkoxy substituents prevent vertical

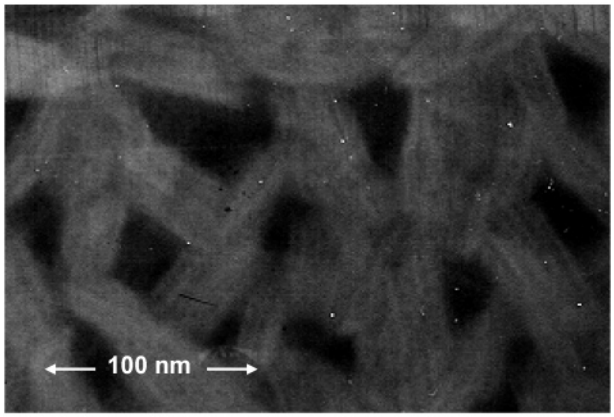

Figure 6. TEM image showing bundles of 5PDI-TAP columnar aggregates cast onto a TEM grid from MCH.

packing of the chromophores and the adjacent 5PDI cores are slipped laterally within a column along their short in-plane axes, is consistent with the SAXS data. It is important to note that the slipping of stacked dyes along their short in-plane axes in the proposed aggregate structure is different from slipping along the long transition moment axis of stacked 5PDI chromophores characteristic of a *J*-type aggregate. A small degree of lateral slipping of adjacent cores (see Figure 5) does not disrupt the coupling of the adjacent, parallel transition dipoles that give rise to the blue-shifted electronic absorption spectra characteristic of *H*-aggregates. It is interesting to note that PDI derivatives analogous to 5PDI-TAP having no bay region substituents, as well as those having 4-alkylphenoxy groups attached to the 1 and 7 positions or to the 1, 6, 7, and 12 positions, exhibit red-shifted optical absorption bands, which are indicative of self-assembly to form *J*-aggregates.[7,8] It is clear that there is a subtle balance between steric interactions of the substituents and the electrostatic interactions of the aromatic core that dictates which type of aggregate is most stable.

Transmission electron microscopy (TEM) was used to characterize films of 5PDI-TAP cast from a preaggregated MCH solution. A 10^{-5} M 5PDI-TAP solution in MCH was cast onto a TEM grid in a solvent-saturated atmosphere. The TEM image in Figure 6 reveals bundles of aggregated 5PDI-TAP molecules that measure several hundred nanometers in diameter. Directional order in thin films is important to preparing efficient OPVs. The image in Figure 6 demonstrates bulk ordering of 5PDI-TAP in thin films that can be optimized for the future development of oriented thin-film materials and devices. The individual parallel stacks of 5PDI-TAP are readily apparent in the TEM image. It is likely that the stacked structures observed in solution by SAXS continue to grow into much larger stacks that eventually associate with nearby stacks as a result of hydrophobic interactions between the long alkyl tails at the periphery of each stack.

Transient absorption measurements were carried out on 5PDI-TAP in MCH and toluene. The data in Figure 7 show that in MCH the bleach of the ground-state absorption band at 630 nm is accompanied by the formation of a 760 nm absorption band, both of which appear within the 0.13 ps instrument response function (IRF) of the experiment. The ground-state bleach shows strong exciton coupling, with a dominant 630 nm band and a weaker 680 nm band. In toluene the ground-state bleach at 700 nm also occurs within the IRF, but the band at 760 nm does not appear. Additionally, the ground-state bleach shows the system is not aggregated in toluene. The redder band at 700 nm is stronger, while the bluer band at 630 nm is weaker.

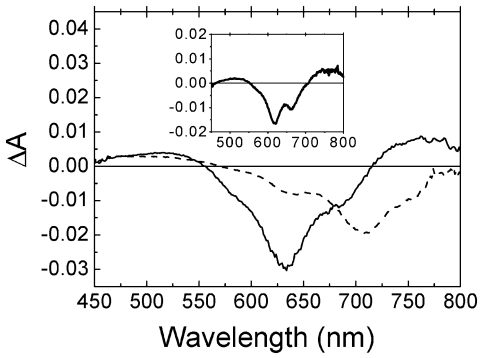

Figure 7. Transient absorption spectra of 5PDI-TAP in MCH (—) and toluene (---) 269 ps after excitation with a 400 nm, 80 fs laser pulse. Inset: transient absorption spectrum of *cof*-5PDI$_2$ in MCH (—) 156 ps after excitation with a 400 nm, 80 fs laser pulse.

The absorption changes of 5PDI-TAP at 630 and 760 nm in MCH both decay with $\tau = 860$ ps, while the 700 nm bleach of 5PDI-TAP in toluene decays with $\tau = 4.5$ ns, the lifetime of the lowest excited singlet state of the 5PDI monomer.[20] The transient absorption spectrum of *cof*-5PDI$_2$ obtained in MCH is shown in the inset to Figure 7. This spectrum is very similar to that of (5PDI-TAP)$_5$ in MCH solution, as evidenced by the absorbance bleach at 630 nm and the positive ΔA feature at 710−800 nm. These transient spectral features both decay with $\tau = 1050$ ps. Our earlier work on *cof*-5PDI$_2$ has shown that the transient absorption feature at 710−800 nm is due to the formation of 5PDI$^{\bullet-}$ that results from excited-state symmetry breaking leading to 5PDI$^{\bullet+}$−5PDI$^{\bullet-}$ with $\tau = 0.52$ ps.[20] The formation of the 760 nm absorption band for both *cof*-5PDI$_2$ and (5PDI-TAP)$_5$ in MCH shows that this same process leads to the formation of 5PDI$^{\bullet+}$−5PDI$^{\bullet-}$ in (5PDI-TAP)$_5$. The differences in charge separation and recombination time constants between the model compound, *cof*-5PDI$_2$, and the self-assembled system, (5PDI-TAP)$_5$, most likely arise from slight variations in the 5PDI−5PDI distances in the self-assembled and covalent scaffold geometries. The faster charge separation and charge recombination rates for (5PDI-TAP)$_5$ may indicate a closer spacing between the chromophores and stronger electronic coupling.

The 5PDI molecule is both a good electron donor and good electron acceptor, having one-electron-oxidation and -reduction potentials of 0.05 and −1.28 V vs Fc/Fc$^+$, respectively, in butyronitrile/0.1 M TBAPF$_6$. On the other hand, the trialkoxyphenyl (TAP) groups at the ends of 5PDI-TAP oxidize at 0.6 V vs Fc/Fc$^+$. Given that the lowest excited singlet state energy of the 5PDI monomer is only 1.75 eV, and that the corresponding energy of (5PDI-TAP)$_5$ is undoubtedly lower due to the exciton interaction between the 5PDI chromophores, intramolecular charge separation to form TAP$^{\bullet+}$−5PDI$^{\bullet-}$ is precluded because $\Delta G > 0$.[44] Thus monomeric 5PDI-TAP should not undergo an internal electron transfer, and is expected to be fluorescent. As a consequence, in polar solvents, this system should be emissive, and in nonpolar solvents (such as MCH) the fluorescence should be quenched by electron transfer between adjacent 5PDI-TAP molecules within the stack. In toluene, which is a disaggregating solvent, the quantum yield of fluorescence is 0.27, which is comparable to the 0.35 quantum yield for 5PDI in toluene,[19] while the fluorescence is completely quenched in MCH.

The similarity in the decay times for the 760 nm 5PDI$^{\bullet-}$ bands in *cof*-5PDI$_2$ and (5PDI-TAP)$_5$ suggests that the initial 5PDI$^{\bullet+}$ and 5PDI$^{\bullet-}$ radical ions produced in the self-assembled 5PDI-TAP pentamers most likely do not separate beyond the adjacent dimeric pair. However, it may be possible that this "bipolaron" may migrate through the structure. These results indicate that the electronic coupling between the π-stacked 5PDI-TAP molecules in MCH is comparable to that enforced by the covalent structure in *cof*-5PDI$_2$. In contrast, 5PDI-TAP dissolved in toluene does not self-assemble into *H*-aggregates, so the cofacial geometry favorable for photoinduced charge separation via excited-state symmetry breaking is not available. Future studies using time-resolved EPR spectroscopy will probe the dynamics of charge transport through these self-assembled structures.

Conclusions

We have demonstrated that we can impose the geometry necessary for excited-state symmetry breaking within a pair of 5PDI molecules through noncovalent solvophobic/dispersive interactions involving the TAP groups. Thus self-assembled materials based on 5PDI-TAP are excellent candidates for further development into components for photovoltaic devices, primarily because of their broad electronic absorption spectra and their ability to quantitatively generate charges as a consequence of symmetry breaking in the excited state following photoexcitation. The 5PDI-TAP aggregates are assembled from a single subunit, which simplifies their overall design and differs from previously reported OPV candidate systems, which are based on mixtures.[1,3,7,16] Our TEM data indicate that 5PDI-TAP retains its structural motif in the solid state, which is an important feature for device applications. Future studies will explore ways to achieve unidirectional order over macroscopic dimensions in the solid, and will probe how to promote long-distance charge migration through these self-assembled materials.

Acknowledgment. This work was supported by the Office of Naval Research (N00014-02-1-0381). The authors thank Drs. D. M. Tiede and A. J. Goshe of the Argonne National Laboratory for assistance in obtaining the SAXS data. This work also made use of facilities supported by the MRSEC program of the National Science Foundation (DMR-0076097) at the Materials Research Center of Northwestern University.

References and Notes

(1) Schmidt-Mende, L.; Fechtenkötter, A.; Müllen, K.; Moons, E.; Friend, R. H.; Mackenzie, J. D. *Science* **2001**, *293*, 1119−1122.

(2) van de Craats, A. M.; Stutzmann, N.; Bunk, O.; Nielsen, M. M.; Watson, M.; Müllen, K.; Chanzy, H. D.; Sirringhaus, H.; Friend, R. H. *Adv. Mater.* **2003**, *15*, 495−499.

(3) Schenning, A. P. H. J.; van Herrikhuyzen, J.; Jonkheijm, P.; Chen, Z.; Würthner, F.; Meijer, E. W. *J. Am. Chem. Soc.* **2002**, *124*, 10252−10253.

(4) Miura, A.; Chen, Z.; Uji-i, H.; De Feyter, S.; Zdanowska, M.; Jonkheijm, P.; Schenning, A. P. H. J.; Meijer, E. W.; Würthner, F.; De Schryver, F. C. *J. Am. Chem. Soc.* **2003**, *125*, 14968−14969.

(5) Neuteboom, E. E.; Meskers, S. C. J.; Van Hal, P. A.; Van Duren, J. K. J.; Meijer, E. W.; Janssen, R. A. J.; Dupin, H.; Pourtois, G.; Cornil, J.; Lazzaroni, R.; Bredas, J.-L.; Beljonne, D. *J. Am. Chem. Soc.* **2003**, *125*, 8625−8638.

(6) Neuteboom, E. E.; Meskers, S. C. J.; Meijer, E. W.; Janssen, R. A. J. *Macromol. Chem. Phys.* **2004**, *205*, 217−222.

(7) van Herrikhuyzen, J.; Syamakumari, A.; Schenning, A. P. H. J.; Meijer, E. W. *J. Am. Chem. Soc.* **2004**, *126*, 10021−10027.

(8) Würthner, F.; Thalacker, C.; Diele, S.; Tschierske, C. *Chem. Eur. J.* **2001**, *7*, 2245−2253.

(9) Cormier, R.; Gregg, B. A. *J. Phys. Chem. B* **1997**, *101*, 11004−11006.

(10) Cormier, R.; Gregg, B. A. *Chem. Mater.* **1998**, *10*, 1309−1319.

(11) Gregg, B. A. *J. Phys. Chem. B* **2003**, *107*, 4688−4698.

(12) Liu, S.-G.; Sui, G.; Cormier, R. A.; Leblanc, R. M.; Gregg, B. A. *J. Phys. Chem. B* **2002**, *106*, 1307−1315.

(13) Struijk, C. W.; Sieval, A. B.; Dakhorst, J. E. J.; van Dijk, M.; Kimkes, P.; Koehorst, R. B. M.; Donker, H.; Schaafsma, T. J.; Picken, S. J.; van de Craats, A. M.; Warman, J. M.; Zuilhof, H.; Sudholter, E. J. R. *J. Am. Chem. Soc.* **2000**, *122*, 11057−11066.

(14) Rohr, U.; Schlichting, P.; Böhm, A.; Gross, M.; Meerholz, K.; Bräuchle, C.; Müllen, K. *Angew. Chem., Int. Ed.* **1998**, *37*, 1434−1437.

(15) Rohr, U.; Kohl, C.; Müllen, K.; van de Craats, A. M.; Warman, J. *J. Mater. Chem.* **2001**, *11*, 1789−1799.

(16) Würthner, F.; Chen, Z.; Hoeben, F. J. M.; Osswald, P.; You, C.-C.; Jonkheijm, P.; Herrikhuyzen, J. v.; Schenning, A. P. H. J.; van der Schoot, P. P. A. M.; Meijer, E. W.; Beckers, E. H. A.; Meskers, S. C. J.; Janssen, R. A. J. *J. Am. Chem. Soc.* **2004**, *126*, 10611−10618.

(17) Ahrens, M. J.; Fuller, M. J.; Wasielewski, M. R. *Chem. Mater.* **2003**, *15*, 2684−2686.

(18) Zhao, Y.; Wasielewski, M. R. *Tetrahedron Lett.* **1999**, *40*, 7047−7050.

(19) Lukas, A. S.; Zhao, Y.; Miller, S. E.; Wasielewski, M. R. *J. Phys. Chem. B* **2002**, *106*, 1299−1306.

(20) Giaimo, J. M.; Gusev, A. V.; Wasielewski, M. R. *J. Am. Chem. Soc.* **2002**, *124*, 8530−8531.

(21) Staab, H. A.; Riegler, N.; Diederich, F.; Krieger, C.; Schweitzer, D. *Chem. Ber.* **1984**, *117*, 246−259.

(22) Kang, T. J.; Kahlow, M. A.; Giser, D.; Swallen, S.; Nagarajan, V.; Jarzeba, W.; Barbara, P. F. *J. Phys. Chem.* **1988**, *92*, 6800−6807.

(23) Rettig, W. *Angew. Chem., Int. Ed. Engl.* **1986**, *25*, 971−988.

(24) Lathrop, E. J. P.; Friesner, R. A. *J. Phys. Chem.* **1994**, *98*, 3056−3066.

(25) Won, Y.; Friesner, R. A. *Proc. Natl. Acad. Sci. U.S.A.* **1987**, *84*, 5511−5515.

(26) Parson, W. W.; Scherz, A.; Warshel, A. *Springer Ser. Chem. Phys. (Antennas React. Cent. Photosynth. Bacteriol.)* **1985**, *42*, 122−130.

(27) Laporte, L. L.; Palaniappan, V.; Kirmaier, C.; Davis, D. G.; Schenck, C. C.; Holten, D.; Bocian, D. F. *J. Phys. Chem.* **1996**, *100*, 17696−17707.

(28) Rybtchinski, B.; Sinks, L. E.; Wasielewski, M. R. *J. Am. Chem. Soc.* **2004**, *126*, 12268−12269.

(29) Percec, V.; Ahn, C.-H.; Bera, T. K.; Ungar, G.; Yeardley, D. J. P. *Chem.—Eur. J.* **1999**, *5*, 1070−1083.

(30) Seifert, S.; Winans, R. E.; Tiede, D. M.; Thiyagarajan, P. *J. Appl. Crystallogr.* **2000**, *33*, 782−784.

(31) Guinier, A.; Fournet, G. *Small Angle Scattering*; Wiley: New York, 1955.

(32) Svergun, D. I.; Koch, M. H. *Rep. Prog. Phys.* **2003**, *66*, 1735−1782.

(33) Svergun, D. I. *J. Appl. Crystallogr.* **1992**, *25*, 495−503.

(34) Svergun, D. I.; Semenyuk, A. V.; Feigin, L. A. *Acta Crystallogr., Sect. A* **1988**, *44*, 244−251.

(35) Svergun, D. I. *Biophys. J.* **1999**, *76*, 2879−2886.

(36) Volkov, V. V.; Svergun, D. I. *J. Appl. Crystallogr.* **2003**, *36*, 860−864.

(37) Rybtchinski, B.; Sinks, L. E.; Wasielewski, M. R. *J. Phys. Chem. A* **2004**, *108*, 7497−7505.

(38) Kasha, M.; Rawls, H. R.; El-Bayoumi, M. A. *Pure Appl. Chem.* **1965**, *11*, 371−392.

(39) Glatter, O. In *Neutron, X-ray and Light Scattering*; Lindner, P., Zemb, T., Eds.; Elsevier: Amsterdam, 1991; pp 33−82.

(40) Glatter, O.; Kratky, O. In *Small-Angle X-ray Scattering*; Academic Press: London, 1982.

(41) Ahrens, M. J.; Sinks, L. E.; Rybtchinski, B.; Liu, W.; Jones, B. A.; Giaimo, J. M.; Gusev, A. V.; Goshe, A. J.; Tiede, D. M.; Wasielewski, M. R. *J. Am. Chem. Soc.* **2004**, *126*, 8284−8294.

(42) Li, X.; Sinks, L. E.; Rybtchinski, B.; Wasielewski, M. R. *J. Am. Chem. Soc.* **2004**, *126*, 10810−10811.

(43) PM3 calculations were performed using HyperChem (TM), Hypercube Inc., 1115 NW 1114th Street, Gainesville, FL 32601.

(44) Weller, A. *Z. Phys. Chem.* **1982**, *133*, 93−98.